

Article



pubs.acs.org/JPCB

Length and Charge of Water-Soluble Peptoids Impact Binding to **Phospholipid Membranes**

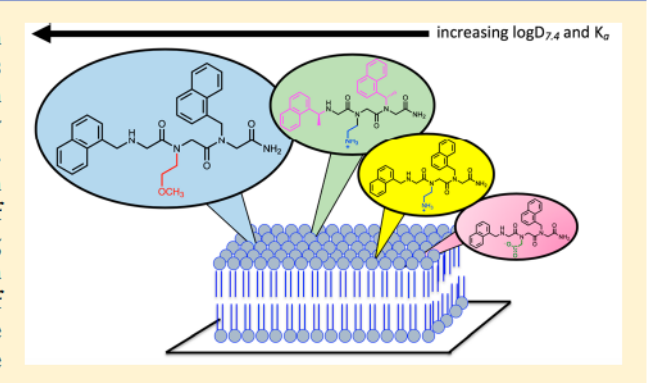
Published as part of The Journal of Physical Chemistry virtual special issue "Pacific Conference on Spectroscopy and Dynamics".

Madeleine R. Landry, Jacenda L. Rangel, Vivian P. Dao, Morgan A. MacKenzie, Fabiola L. Gutierrez, Kalli M. Dowell, Anna L. Calkins, Amelia A. Fuller, and Grace Y. Stokes*

Department of Chemistry and Biochemistry, Santa Clara University, 500 El Camino Real, Santa Clara, California 95053, United States

Supporting Information

ABSTRACT: In this study, we provide a quantitative description of the adsorption of water-soluble N-substituted glycine oligomers (peptoids) to supported lipid bilayers that mimic mammalian plasma membranes. We prepared a small array of systematically varied peptoid sequences ranging in length from 3 to 15 residues. Using the nonlinear optical method second harmonic generation (SHG), we directly monitored adsorption of aqueous solutions of 3- and 15-residue peptoids to phospholipid membranes of varying physical phase, cholesterol content, and head group charge in physiologically relevant pH buffer conditions without the use of extrinsic labels. Equilibrium binding constants and relative surface coverages of adsorbed peptoids were determined from fits to the Langmuir model. Three- and 15-residue peptoids did not interact



with cholesterol-containing lipids or charged lipids in the same manner, suggesting that a peptoid's adsorption mechanism changes with sequence length. In a comparison of four three-residue peptoids, we observed a correlation between equilibrium binding constants and calculated log D_{7.4} values. Cationic charge modulated surface coverage. Principles governing how peptoid sequence and membrane composition alter peptoid-lipid interactions may be extended to predict physiological effects of peptoids used as therapeutics or as coatings in medical devices.

■ INTRODUCTION

Small organic molecules may adsorb to and perturb the physical structure of lipids in the mammalian plasma membrane (PM), causing changes to the conformation and function of transmembrane proteins. 1,2 These nonspecific interactions can result in physiological effects related to drug bioaccumulation and toxicity.3 Predictive models describing how changes to chemical structure alter membrane association are available for a limited library of small molecule drugs and organic pollutants.⁴⁻⁹ To develop these models further, more data are needed for molecules bearing a wide range of functionalities.

Peptoids, N-substituted glycine oligomers (Figure 1), can be methodically varied to provide a range of diverse structures. 10,11 Peptoids are peptidomimetics in that they maintain the amide backbone of peptides, but the side chain substituents (R-groups) are connected to the amide nitrogen instead of the α-carbon atom. 12-15 A variety of functionality can be included to generate peptoid residues that are aromatic ((S)-N-(1naphthylethyl)glycine, Ns1npe; N-(1-naphthylmethyl)glycine, N1npm; N-(phenylmethyl)glycine, Npm), cationic (N-(2aminoethyl)glycine, Nae), neutral polar (N-(2-methoxyethyl)- glycine, Nme), or anionic ((S)-N-(1-carboxyethyl)glycine,Nsce; N-(carboxymethyl)glycine, Ncm). Further, chiral, sterically bulky $N-\alpha$ -substituted residues can be installed (e.g., Ns1npe, Nsce). Unlike peptides, peptoids lack backbone intramolecular hydrogen bond donors and have an achiral backbone. Peptoids have been shown to permeate bacterial membranes and exhibit antibacterial and antifouling properties. 16-21 In the human body, peptoids are less prone to enzymatic degradation compared to peptides and proteins. 22,23 Owing to these favorable properties, a number of investigators screened peptoid libraries and discovered structures with other therapeutic effects.²⁴⁻²⁸

Given the promising applications of peptoids and the structure-property insights which can be gained from their study, a molecular-level understanding of how peptoids interact with phospholipids, the primary component of mammalian PMs, is needed. A limited number of reports have detailed peptoid-lipid interactions through studies of

Received: May 15, 2019 Revised: June 13, 2019 Published: June 17, 2019



(A) Representative tripeptoid

$$R_3 \stackrel{H}{\stackrel{\bigcirc}{\bigvee}} \stackrel{O}{\stackrel{\longrightarrow}{\bigvee}} \stackrel{R_1}{\stackrel{\bigcirc}{\bigvee}} \stackrel{O}{\stackrel{\longrightarrow}{\bigvee}} NH_2$$

(B) Residues used in this study, R =

aromatic:

Figure 1. (A) Side chain substituents (R-groups) are connected to amide nitrogen in a peptoid. (B) R-groups of varying hydrophobicity and charge used in this study. Residue abbreviations are listed below R-group structures as elaborated in the text.

peptoid interactions with cells, liposomes, and bicelles. Previous studies have highlighted the importance of hydrophobic residues for peptoids' selective interactions with bacterial versus mammalian membranes. 17,21 Further, thermodynamic forces driving interactions of peptoids with liposomes varied slightly on the basis of the size and hydrogen bonding capacity of substituents.^{29,30} Peptoids have also exhibited different localization within bicelles.31 However, the mechanisms by which peptoids incorporate into natural or artificial PMs are not fully understood.3

In this study, we monitored adsorption of aqueous solutions of water-soluble peptoids to artificial PMs using the nonlinear optical method, second harmonic generation (SHG),33 which offers a number of advantages. Label-free detection is particularly important given that fluorophore labeling of either the adsorbate (here, the peptoid)³⁶ or lipid³⁷ has been shown to change the mechanism and strength of phospholipid interactions. SHG enables label-free detection; it was previously used to study small molecule drug-phospholipid interactions without the use of extrinsic tags. 38-40 Additionally, SHG enabled us to directly quantify both the strength of adsorption and the relative surface coverage to gain insight into the mechanism of adsorption.

In this study, we monitored interactions between peptoids and supported lipid bilayers (SLBs), the latter of which were used to mimic the thickness, structure, and lateral fluidity of mammalian PMs. We systematically varied fluidity and cholesterol content of the lipid bilayer, as well as the charge of the lipid head group to discover the membrane characteristics that modulate peptoid-lipid interactions. We also investigated the impacts of peptoid length, charge, and side chain composition within a library of related structures on binding affinities to lipids and membrane concentrations. These findings begin to clarify sequence-function relationships that may be important for further development of biologically active peptoids.

EXPERIMENTAL METHODS

Peptoid Synthesis. Reagents for peptoid synthesis were purchased from commercial suppliers and used without further purification. Fmoc-protected Rink amide resin was purchased

from EMD Millipore. Solvents were purchased from Fisher Scientific unless otherwise specified. The 15- and 6-residue peptoids (1 and 2, respectively) used in this study were synthesized and purified according to previously published procedures. 41 Eight tripeptoids were prepared following an analogous synthetic strategy, also previously published.⁴² New peptoids reported in this study (3, 4, 5, 6) were identified by electrospray mass spectrometry in positive ion mode using an Agilent 1260 Infinity II LC with a 6230 time-of-flight mass spectrometer (TOF MS) detector (electrospray ionization, positive ion mode) and were within 5 ppm of expected values (Supporting Information, Table S1). UV-vis spectra of three representative peptoids are shown in Figure S1.

Peptoid Solution Preparation. Phosphate buffered saline (PBS buffer) was prepared with 50 mM sodium phosphate (Fisher Scientific) using ultrapure 18 M Ω water (Thermo-Scientific Barnstead Micropure). The pH of the PBS buffer was adjusted to either 6.2, 7.4, or 8.2, as indicated, with sodium hydroxide (Macron) or hydrochloric acid (EMD). Total ionic strength (IS) was maintained at 0.215 M using sodium chloride (Alfa Aesar). All buffers were stored at 4 °C for up to one month. A solution of 50 mM HEPES buffer was prepared by dissolving 4-(2-hydroxyethyl)-1-piperazineethanesulfonic acid (99%, Fisher) in ultrapure 18 M Ω water and adding 193 mM sodium chloride to reach IS = 0.215 M, and the pH was adjusted to 7.4 by addition of sodium hydroxide (Macron). Concentrated peptoid stock solutions were prepared by dissolving lyophilized peptoids in HPLC grade (99.8%) methanol (Alfa Aesar) with concentrations ranging from 2×10^{-3} to 2×10^{-2} M, and stored at 4 °C. Aqueous peptoid dilutions with concentrations ranging from 1×10^{-7} to 4×10^{-5} M were prepared with PBS or HEPES buffer, as specified, at the beginning of each adsorption isotherm experiment by addition of appropriate volumes of the stock peptoid solution to PBS or HEPES buffer so that the final methanol content always remained below 2%.

Lipid Bilayer Preparation. 1,2-Dioleoyl-sn-glycero-3phosphocholine (DOPC), 1,2-dimyristoyl-sn-glycero-3-phosphocholine (DMPC), 1,2-dipalmitoyl-sn-glycero-3-phosphocholine (DPPC), 1,2-dioleoyl-sn-glycero-3-phospho-(1'-racglycerol) (DOPG), and 1,2-dioleoyl-3-trimethylammoniumpropane (chloride salt) (DOTAP) were purchased from Avanti Polar Lipids. Cholesterol (≥99%) was purchased from Sigma-Aldrich and used as received. (Structures of lipids are shown in the Supporting Information, Figure S2.) Chloroform (HPLC grade) was purchased from Honeywell Burdick and Jackson. Dried lipid films were prepared by combining the appropriate volumes of stock lipids, as received from the supplier in chloroform, and mixed by vortexing. The lipid mixture solutions were evaporated under a gentle stream of nitrogen gas (ultrahigh purity, Matheson) and vacuum-dried overnight to remove residual chloroform. Dried lipid aliquots (1 mg) were stored at -20 °C. Supported lipid bilayers (SLB) were prepared by spontaneous rupture and fusion of small unilamellar vesicles (SUVs) to a clean fused silica prism substrate (cleaning procedures described below) following established protocols.⁴³ SUVs were prepared by reconstituting dried lipids with 2 mL of PBS pH 7.4 (final lipid concentration of 0.5 mg/mL) followed by vortexing to mix and bath sonication for 20 min, or until solutions changed from turbid to clear. Saturated lipids required heating to a temperature ~10 $^{\circ}$ C above the phase transition temperature (T_m) before SUV solutions were injected into the flow cell (volume ~0.5 mL).

Lipids were allowed to equilibrate with the silica prism substrate for 20 min. A minimum of 10 mL of PBS pH 7.4 (10 times the volume of the flow cell) was injected into the flow cell to remove unbound lipids. When buffers other than PBS pH 7.4 were used, the buffers were exchanged after the formation of the SLB and rinsed with 10 mL of PBS pH 7.4. Buffer exchange involved rinsing the flow cell through with at least three 10 mL portions of 50 mM HEPES or PBS pH 6.2 or PBS pH 8.2. This volume of solution was 30 times the volume of the flow cell (~1 mL).

Second Harmonic Generation (SHG) Theory. In SHG, a photon with frequency 2ω is generated when two photons of frequency ω are spatially and temporally overlapped at an interface. Within the electric dipole approximation, peptoids dissolved in aqueous solution are isotropically distributed and do not generate an SHG signal. A separation step is not required to isolate signal from peptoids adsorbed to the SLB because the SHG signal is surface specific and only molecules adsorbed to an interface (where symmetry is necessarily broken), such as at the liquid/solid interface where the SLB is located, contribute to changes in SHG intensities. 34,35 SHG intensity is proportional to N^2 (eq 1), the square of the number of molecules adsorbed to the interface.

$$\begin{split} I_{\text{SHG}} & \propto |\chi_{\text{NR}}^{(2)} + \chi_{\text{R}}^{(2)}|^2 \\ & \propto \left| \chi_{\text{NR}}^{(2)} + N \sum_{a,b,c} \frac{\langle a|\mu_i|c\rangle\langle a|\mu_j|b\rangle\langle b|\mu_k|c\rangle}{(2\hbar\omega - E_{ca} - i\Gamma_{ca})(\hbar\omega - E_{ba} - i\Gamma_{bc})} \right|^2 \end{split}$$

In eq 1, $\chi_R^{(2)}$ is the resonant contribution, and $\chi_{NR}^{(2)}$ is the nonresonant contribution to second order susceptibility. h is Planck's constant, and μ is the Cartesian coordinate dipole operator. Γ represents the line width for the transition, and subscripts a, b, and c are the initial, intermediate, and final states, respectively. Resonantly enhanced SHG signal can be generated when the frequency of the incident (ω) or second harmonic (2ω) light approaches the frequency of an inherent electronic transition of a molecule located at the liquid/solid interface, E_{ba} or E_{car} respectively.

SHG Experimental Setup. SHG was used to monitor the adsorption of aqueous peptoid solutions to SLBs. SHG experiments were performed with a Q-switched Nd:YAG laser with a 7 ns pulse width at a repetition rate of 10 Hz (Surelite III-EX, Continuum) in a counterpropagating geometry.^{39,40,44} A type 1 (SD-1) doubling crystal was used to produce 532 nm laser light, which was directed onto the surface of the fused silica prism (Almaz Optics, UV-grade SiO2, KU-1) at an angle of 67° under total internal reflection and steered onto the surface of a high-energy Nd:YAG mirror (Thorlabs, KB1-K12). The final collimated beam with a diameter of 4 mm and an intensity of 20 mJ/pulse was spatially overlapped with the incident laser light to produce SHG light perpendicular to the silica prism surface. The SHG signal was passed through two single-band bandpass filters (Semrock, FF01-260 and LL01-266) and detected with a photomultiplier tube (Hamamatsu R7154).

Flow Cell Cleaning Procedures. The chlorotrifluoroethylene (CTFE) flow cell was connected to tetrafluoroethylene (TFE) tubing via polytetrafluoroethylene (PTFE) inlet and outlet connectors. A Teflon O-ring (Hydrapak, 2-015 V/TE) was pressed between the silica prism substrate and the CTFE flow cell to ensure a water-tight seal. The silica prism

substrate and all flow cell components were cleaned in piranha etch, a 70:30 v/v solution of 18 M sulfuric acid (VWR) and 30% hydrogen peroxide (VWR) overnight. (CAUTION: This solution is a strong oxidant and reacts violently with organic solvents. Extreme caution must be taken when handling this solution.) Prior to each experiment, the silica prism substrate and all flow cell components were removed from piranha etch and rinsed with copious amounts of ultrapure 18 $M\Omega$ water. The silica prism substrate was plasma cleaned (Harrick Scientific) for 3 min immediately before it was mounted to the flow cell.

SHG Isotherm Collection Procedure. To ensure that peptoid concentration in the bulk phase was not depleted by adsorption, at least three 3 mL injections of the same peptoid concentration were introduced into the flow cell for concentrations ranging from 1×10^{-6} to 5×10^{-6} M. After each injection, at least 30 min were allotted to allow equilibration with the lipid bilayer. Higher concentrations of peptoid above 10×10^{-6} M were injected through one 4 mL injection and equilibrated with the lipid bilayer for at least 30 min. The equilibration durations were sufficient for detecting a steady-state SHG response. All isotherms were collected at room temperature.

SHG Isotherm Collection and Normalization Procedure. SHG signal intensities were averaged from three separate isotherm experiments conducted on three different days and normalized using the following two-point normalization method: 40 SHG intensities from (1) 0.01 M potassium hydroxide (Macron) and (2) PBS buffer pH 7.4 adsorbed to bare silica were measured at the end of each laser experiment and used to correct for changes in collection efficiency and day-to-day laser fluctuations (including differences in the intensity of the incident laser light). Normalized SHG isotherm data were fit to a simplified form of the Langmuir equation (eq 2), which assumes that $\chi_{\rm R}^{(2)}$ is significantly larger than $\chi_{\rm NR}^{(2)}$ (see eq 1 above) and is therefore the dominant contributor to $I_{\rm SHC}$.

$$I_{\text{SHG}} \propto \left(\frac{\sqrt{I_{\text{SHG}}^{\text{max}}} K_{\text{a}}[\text{peptoid}]}{1 + K_{\text{a}}[\text{peptoid}]} \right)^{2}$$
 (2)

A detailed derivation of eq 2 based on the Langmuir model, ⁴⁶ taking into account the simplifying assumptions of resonantly enhanced SHG (see eq 1 above), is described in the Supporting Information. Fit coefficients for the equilibrium binding constants (K_a) and SHG intensity at saturation ($I_{\rm SHG}^{\rm max}$) were determined from eq 2. $I_{\rm SHG}^{\rm max}$ values provide a measure of relative surface coverage, because $I_{\rm SHG}$ is proportional to the number of adsorbed peptoids at the interface squared (N^2). One assumption of the Langmuir model is that adsorption is fully reversible. ⁴⁶ Even when this is not the case, the Langmuir model can still be used to describe adsorption of low aqueous concentrations of peptoids if a quasiequilibrium state is assumed to exist during the initial adsorption event at low surface coverage. ⁴⁴

RESULTS AND DISCUSSION

We first examined the adsorption of peptoids with different lengths to SLBs with varied compositions. Although peptoid length has been correlated with selective peptoid interactions with bacterial versus mammalian cellular lipid membranes, the contributions of sequence length to the mechanisms of

1 Nae-Ns1npe-Nsce-Nsce-Ns1npe-Nae-Nae-Ns1npe-Nsce-Nsce-Ns1npe-Nae-Nae-Ns1npe-Nsce

2 Nsce-Ns1npe-Nae-Nae-Ns1npe-Nsce

3 Ns1npe-Nae-Ns1npe

Figure 2. Structures of peptoids with 15 (1), 6 (2), and 3 (3) residues evaluated for adsorption to SLBs. Abbreviations for peptoid sequences are listed below each structure.

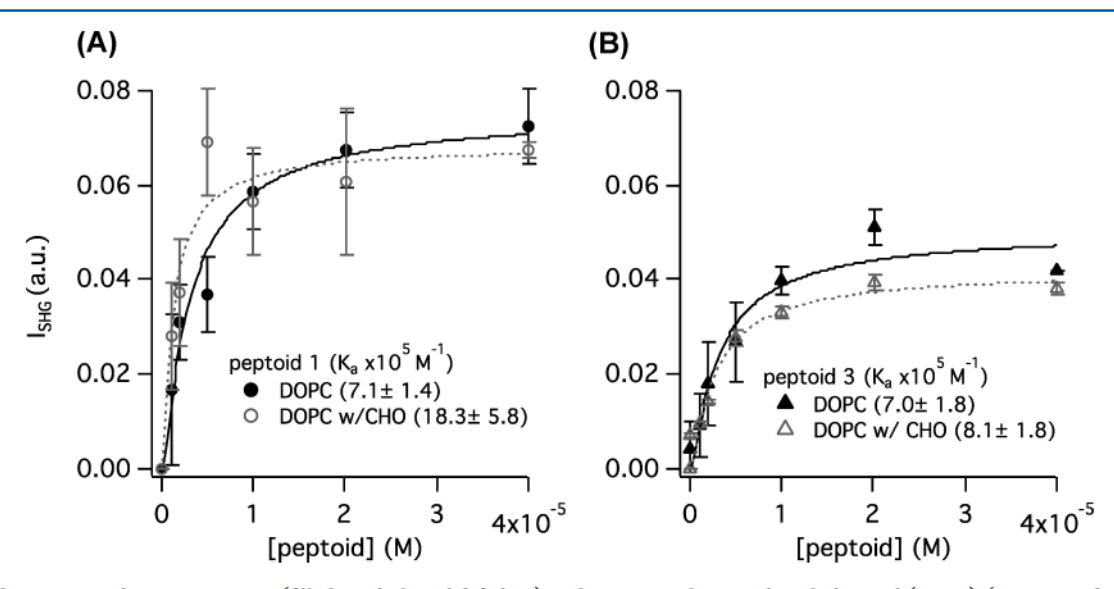


Figure 3. Adsorption isotherms to DOPC (filled symbols, solid fit line) and DOPC with 30 mol % cholesterol (CHO) (empty symbols, dashed fit line) for 15-residue 1 (panel A) and 3-residue 3 (panel B). Equilibrium binding constants (K_a) determined from Langmuir model (eq 2) are shown in parentheses.

peptoid—lipid interactions have not been clarified. ¹⁷ In similar systems, α -peptide/ β -peptoid hybrids, enthalpies and Gibbs free energies of adsorption were more favorable and cellular uptake increased as sequence length increased. ³⁰ These studies underscored the likely importance of hydrophobic interactions in the adsorption of peptoids to lipid bilayers. ³⁰ However, the mechanisms of peptoid—lipid interactions as a function of sequence length have not been fully explored. Furthermore, no previous studies have compared peptoid adsorption to gelversus fluid-phase, cationic versus anionic, or cholesterol-rich versus cholesterol-poor lipids.

Peptoids Designed for Resonantly Enhanced SHG Signal. With these considerations in mind, we evaluated the adsorption of three peptoids with varied length (Figure 2) to

SLBs of varied compositions. Each peptoid we studied contained at least one aromatic residue, Ns1npe. Peptoids bearing these residues were particularly well-suited for SHG studies because they exhibited strong absorbances around the SHG wavelength of 266 nm (Figure S1). Peptoids 1 and 2, both studied previously, tomprise a repeating pattern of three residues: Ns1npe, Nsce, and Nae. Peptoids 1 and 2 are predicted to have a net positive charge at neutral pH and to adopt amphiphilic helix structures. Tripeptoid 3 is not a direct analogue of 1 or 2 but comprises two Ns1npe in terminal positions and one central Nae residue and is also expected to have a net positive charge. As shown in Figure 2, 1, 2, and 3 have varied numbers of Ns1npe residues; more Ns1npe residues resulted in higher molar absorptivity (Figure S1).

HPLC retention is one experimental measure of hydrophobicity. As the peptoid length increases in the order 3 < 2 < 1, HPLC retention times increase in the same order (Table S2), suggesting that longer peptoids are more hydrophobic.

We predicted that adsorption of peptoids with 15 residues or fewer would behave like that of small organic molecules, which adsorbed to fluid-phase DOPC with higher binding affinities and surface coverage than to gel-phase DPPC lipids. Therefore, we first distinguished which peptoids adsorbed to DOPC at pH 7.4 in PBS buffer. For those peptoids which adsorbed to DOPC, we additionally monitored adsorption to gel-phase lipids such as DMPC and DPPC. We also examined the contributions of head group charge and cholesterol to peptoid—lipid interactions. We monitored adsorption to DOPC doped with 30 mol % cholesterol (DOPC w/CHO), DOPC doped with 10% DOTAP (+), and DOPC doped with 10% DOPG (—). (Chemical structures of all lipids used in SHG experiments are shown in Supporting Information Figure S2.)

Peptoids 1 and 3 Adsorbed to DOPC but 2 Did Not. We compared binding properties of 1, 2, and 3, which have 15, 6, and 3 total residues, respectively. Despite differences in length, sequence, and 3-D structure, 1 and 3 adsorbed to DOPC with similar K_a values of $7.1 \pm 1.4 \times 10^5$ and 7.0 ± 1.8 \times 10⁵ M⁻¹, respectively (Figure 3). These K_a values were consistent with equilibrium constants reported for α -peptide/ β -peptoid hybrids adsorbed to liposomes determined by isothermal calorimetry (ITC), which ranged from 2.9 ± 0.4 \times 10⁵ to 11.8 \pm 0.3 \times 10⁵ M⁻¹ and increased with peptoid length.³⁰ Polarization-resolved SHG experiments suggested that increases in SHG intensities shown in Figure 3 were attributed to higher numbers of adsorbed peptoids (N), not due to changes in orientation of the adsorbed peptoid as surface concentrations increased (Table S3). Complementary fluorescence microscopy experiments showed no evidence of pore formation nor evidence of lipid bilayer degradation or removal at these aqueous peptoid concentrations (Figure S4). Interestingly, intermediate length 2 did not bind to DOPC (Figure S5). Coupled with results described below, this observation indicates that the mechanism of adsorption is length-dependent despite the similar K_a values of 1 and 3.

Adsorption of 1 to DOPC Was Not Fully Reversible. Adsorption of 3 to DOPC was fully reversible, while adsorption of 1 was not (Figures S6 and S7, respectively). Previous studies of 1 in aqueous solution 41,44 suggested self-association of its helical structure, and we speculated that these structural features contributed to a more complex binding interaction compared to that for shorter sequence 3.41,48 The shape of the isotherm data shown in Figure 3A suggested simple Langmuir behavior and did not warrant a more complex binding model.49 No evidence of cooperative behavior50 or of electrostatic interactions51 between peptoids and DOPC in PBS buffer at pH 7.4 was observed.

Longer Peptoid 1 Adsorbed with Higher K_a to DOPC in the Presence of Cholesterol (CHO). Longer peptoid 1 exhibited a 2.6-fold increase in K_a in the presence of 30 mol % CHO (Figure 3), but shorter peptoid 3 exhibited nearly identical K_a values in either the presence or absence of CHO. CHO is found in the plasma membranes of mammalian cells at concentrations as high as 50 mol % and alters the physical structure of lipid bilayers. Although CHO generally has an ordering or condensing effect on acyl chains in fluid-phase lipids, resulting in less space for small organic molecules to

intercalate, ^{53,54} preferential adsorption of tryptophan-rich peptides to CHO-rich domains has been reported. ⁵⁵ In the current studies, the presence of 30 mol % CHO in DOPC resulted in a 5% and 9% decrease in relative surface coverage (θ) at saturation for 1 and 3, respectively (Table 1). θ

Table 1. SHG Signal Intensities at Saturation Determined from Langmuir Fit ($I_{\rm SHG}^{\rm max}$) and Relative Surface Coverages ($\theta = N/N_{\rm DOPC}$) for 1 and 3 Adsorbed to Zwitterionic DOPC, DOPC Doped with 30 mol % CHO, DOPC Doped with 10% DOPG (-), and DOPC Doped with 10% DOTAP (+)^a

	peptoid 1		peptoid 3		
	I _{SHG} (a.u.)	θ	I _{SHG} (a.u.)	θ	
DOPC	0.076 ± 0.005	1	0.051 ± 0.004	1	
DOPC w/CHO	0.068 ± 0.005	0.95	0.042 ± 0.003	0.91	
DOTAP (+)	low^b	low^b	0.029 ± 0.004	0.75	
DOPG (-)	0.034 ± 0.002	0.67	low^b	low^b	

 $^aN/N_{\mathrm{DOPC}}$ was calculated by comparing $\sqrt{I_{\mathrm{SHG}}^{\mathrm{max}}}$ for designated peptoid/lipid combination versus $\sqrt{I_{\mathrm{SHG}}^{\mathrm{max}}}$ of that same peptoid adsorbed to DOPC. $^b\mathrm{Changes}$ in SHG signal too low to calculate fit coefficients.

= $N/N_{\rm DOPC}$ was calculated by comparing $\sqrt{I_{\rm SHG}^{\rm max}}$ for designated peptoid/lipid combination versus $\sqrt{I_{\rm SHG}^{\rm max}}$ of that same peptoid adsorbed to DOPC, because as shown in eq 1, $\sqrt{I_{\rm SHG}^{\rm max}} \propto N$. In previous studies, CHO decreased the bilayer penetrating effects of antimicrobial peptides having a similar length. ⁵⁶

Neutral Form of 1 Bound to Zwitterionic DOPC. Trends in relative surface coverages (θ , which is determined from I_{SHG}^{max}) are expected to be driven by van der Waals or hydrophobic interactions. These interactions are strongest between a neutral peptoid and a zwitterionic lipid such as DOPC. To better understand the impact of the peptoid's ionization state on θ , we monitored adsorption of 1 to DOPC in PBS pH 6.2 and PBS pH 8.2 buffers (Figure S8). These data were fit to the Langmuir model. At different pH conditions, IS was maintained at 0.215 M by addition of appropriate amounts of NaCl. Higher concentrations of the neutral form of 1 are present at pH 8.2, while at pH 6.2, the cationic form of 1 is dominant. Both K_a and I_{SHG}^{max} of 1 at pH 8.2 were higher than at pH 6.2, suggesting that the neutral form of 1 adsorbed with higher affinity and surface coverage to DOPC (Figure S8). Results for 1 corroborate previous reports that the neutral form of a small molecule drug, not the ionized form, was responsible for binding to zwitterionic DOPC.39

Adsorption of 1 and 3 to Charged Lipids Did Not Follow the Same Trends. At pH 7.4, both 1 and 3 possess cationic charge, yet adsorbed with higher $I_{\rm SHG}^{\rm max}$ to zwitterionic DOPC than to charged lipids (Table 1). The 3-fold higher $K_{\rm a}$ value for 1 adsorbed to DOPG (–) compared to DOPC (Figure 4A) may be attributed to electrostatic attractions between the positively charged form of 1 and the anionic lipid. Stronger interactions between 1 and DOPG (–) and weaker interactions between 1 and DOTAP (+) (relative to zwitterionic DOPC) followed expected trends due to electrostatic attraction versus repulsion, respectively. Even though SLBs were prepared following published protocols and 2-D lateral fluidity had been previously quantified, 57,58 absolute differences between DOPC, DOTAP, and DOPG could not be definitively attributed to only electrostatic interactions.

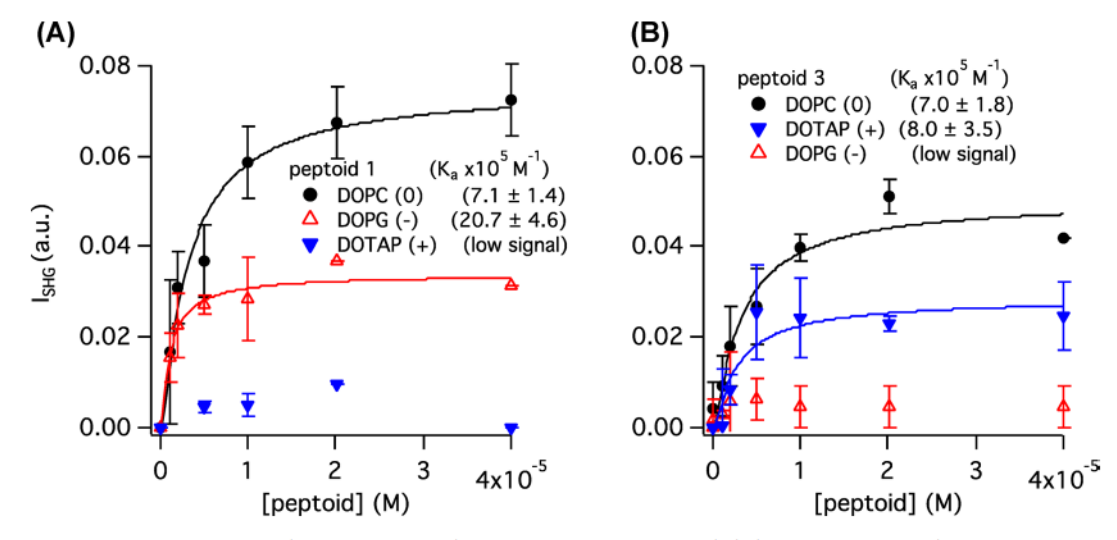


Figure 4. Adsorption isotherms to DOPC (filled black circles), DOPC with 10% DOPG (-) (empty red triangles), and DOPC with 10% DOTAP (+) (filled blue triangles) for 1 (panel A) and 3 (panel B). Equilibrium binding constants (K_a) determined from Langmuir model (eq 2) are shown in parentheses.

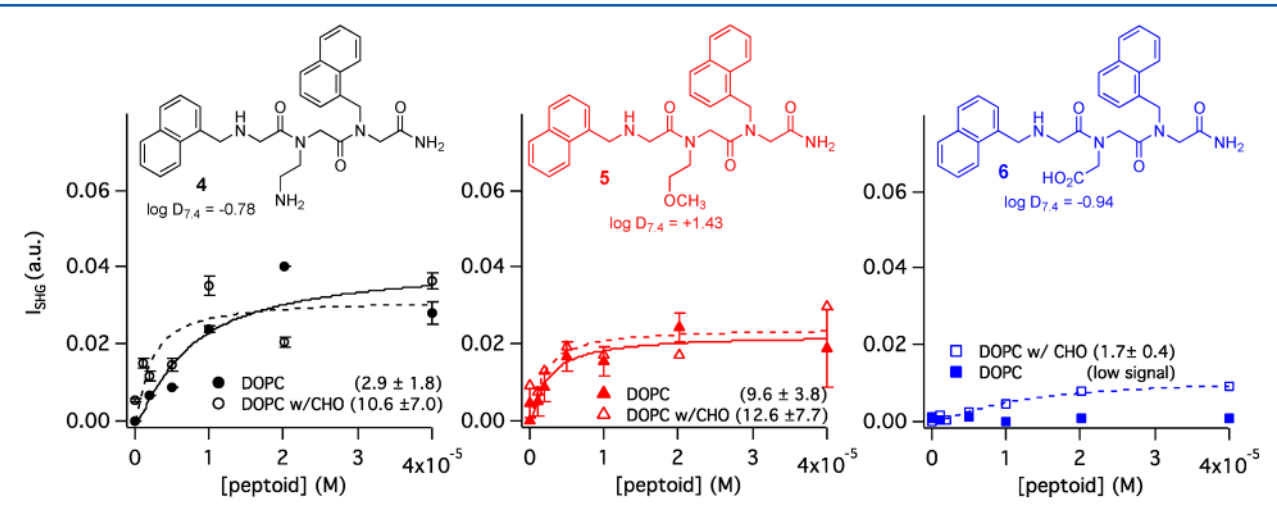


Figure 5. Adsorption isotherms to DOPC (filled symbols, solid fit line) and DOPC with 30 mol % cholesterol (CHO) (empty symbols, dashed fit line) for tripeptoids 4 (panel A), 5 (panel B), and 6 (panel C) with corresponding chemical structures. Experiments were conducted in PBS buffer at pH 7.4. Equilibrium binding constants ($K_4 \times 10^5 \text{ M}^{-1}$) determined from simplified Langmuir model (eq 2) are shown in parentheses.

Previous studies suggested that increased concentrations of charged lipids may change the lateral mobility and packing densities of SLBs. ⁵⁹ However, because SLB preparations were consistent among different peptoids, we expected trends between DOPC, DOTAP, and DOPG to be the same between 3 and 1 and were surprised to observe that they were not.

Shorter peptoid 3 had a higher net cationic charge compared to 1. This cationic charge was confined to a smaller molecular volume, resulting in a higher charge density. K_a values for 3 adsorbed to DOTAP (+) and zwitterionic DOPC were comparable, but $I_{\rm SHG}^{\rm max}$ was lower for the adsorption of 3 to DOTAP (+). The 25% lower θ between cationic 3 and DOTAP (+) versus DOPC (0) may be attributed to charge repulsion. Surprisingly, 3 did not adsorb to DOPG (-), despite the predicted electrostatic attraction between negatively charged lipid and positively charged 3 (Figure 4B). We speculated that because cationic charge is confined to a smaller molecular volume in 3 compared to a larger, helical structure in 1, different modes of interaction are observed for 1 and 3 adsorbed to the same charged lipids. Differences in (1) reversibility of adsorption to DOPC, (2) impact of CHO on

adsorption to DOPC, and (3) interactions with charged lipids all are consistent with different modes of phospholipid binding for peptoids of varying length.

Tripeptoid Adsorption to DOPC and DOPC w/CHO Governed by Hydrophobicity. To determine whether other tripeptoids also behave like 3, we prepared and surveyed seven other tripeptoids for adsorption to DOPC and/or DOPC w/ CHO. Tripeptoids 4, 5, and 6 (Figure 5) contained a varied central residue, Nae, Nme, or Ncm, respectively, and N1npm residues at the terminal positions. The tripeptoids' net cationic charge decreased in the following order: 3 = 4 > 5 > 6. Within this series of structurally similar tripeptoids, we also compared calculated values for the distribution coefficient at pH 7.4 (log $D_{7.4}$), a prediction of partitioning of a molecule between aqueous and lipophilic environments, taking into account the compound's ionization at pH 7.4.60 Calculated log $D_{7.4}$ values were made using ChemAxon's MarvinSketch Calculator Plugin. Although it is not listed in Figure 5, the calculated $\log D_{7.4}$ for tripeptoid 3 is -0.01; thus, tripeptoids' $\log D_{7.4}$ values decreased in the following order: 5 > 3 > 4 > 6. Comparisons of predicted log D_{7.4} values⁶⁰ have previously

Table 2. I_{SHG}^{max} and Surface Coverages Relative to 3 Adsorbed to DOPC ($\theta_3 = N/N_{DOPC forpeptoid3}$) for 4, 5, and 6 Adsorbed to DOPC and DOPC w/CHO^a

	peptoid 4		peptoid 5		peptoid 6	
	I _{SHG} (a.u.)	θ_3	I _{SHG} (a.u.)	θ_3	I _{SHG} (a.u.)	θ_3
DOPC	0.031 ± 0.010	0.78	0.022 ± 0.002	0.66	low signal ^b	low signal ^b
DOPC w/CHO	0.032 ± 0.006	0.79	0.024 ± 0.004	0.69	0.012 ± 0.001	0.49

^aNote that $\sqrt{I_{\rm SHG}^{\rm max}} \propto N$ so $N_{\rm DOPC for peptoid 3}$ was evaluated from $\sqrt{I_{\rm SHG}^{\rm max}}$ for 3 adsorbed to DOPC (top right cell in Table 1). Experiments were conducted at room temperature in PBS buffer at pH 7.4. ^bAbsorbance was too low to calculate fit coefficients.

been used to estimate membrane partitioning of other tripeptoids. ²¹

Relative Surface Coverage of Tripeptoids Modulated by Charge. Tripeptoids 4, 5, and 6 all adsorbed to either DOPC and/or DOPC w/CHO (Figure 5). On the basis of its log D7.4 value, 6 is also the least hydrophobic and had the lowest cationic charge of the three related structures. As shown in Figure 5 and Table 2, 6 exhibited the lowest K_a and lowest relative surface coverage (θ_3). In Table 2, $\theta_3 = N/$ $N_{
m DOPC for peptoid 3}$ was calculated by comparing $\sqrt{I_{
m SHG}^{
m max}}$ for a designated peptoid/lipid combination versus $\sqrt{I_{\rm SHG}^{\rm max}}$ of that tripeptoid 3 adsorbed to DOPC. Among all the tripeptoids studied, 5 had the highest $\log D_{7.4}$ value and was predicted to be the most hydrophobic structure. Fits of the data shown in Figure 5 to the Langmuir adsorption model suggest that 5 adsorbed to DOPC w/CHO exhibited the highest Ka value among all tripeptoid/lipid combinations. However, lower overall SHG signal intensities were exhibited by 4, 5, and 6, and larger errors in the fits were observed; these errors made comparisons of K_a more challenging. Of the four tripeptoids, 3 had the highest cationic charge due to its central Nae residue (equal charge to 4). Peptoid 3 adsorbed to DOPC exhibited the highest I_{SHG} among all other tripeptoid/lipid combinations. Peptoid 4 had a higher cationic charge compared to that of 5 and exhibited 29% and 25% higher θ_3 when adsorbed to DOPC and DOPC w/CHO, respectively. In summary, for tripeptoids, K_a trends followed hydrophobicities (5 > 3 > 4 > 6) while trends in I_{SHG}^{max} followed cationic charge (3 = 4 > 5 > 6).

While the neutral form of 1 adsorbed most strongly to zwitterionic DOPC, 6, which has the lowest cationic charge, exhibited weaker interactions (based on both K_a and θ_3) with zwitterionic DOPC and DOPC w/CHO compared to 4 and 5. It appears that the low hydrophobicity of 6 made interactions with zwitterionic lipid bilayers less favorable despite its lower net charge compared to those of 4 and 5. Thus, tripeptoids 4, 5, and 6 did not follow the trend observed for 1. One feature shared by 4, 5, and 6 and longer peptoid 1 was that K_a and θ_3 were higher for adsorption to DOPC w/CHO than to DOPC alone (Figure 5 and Table 2). We speculated that, like 1, tripeptoids 4, 5, and 6 may preferentially adsorb to the cholesterol-rich domains of the bilayer. 55

Tripeptoids That Lacked Two N1npm Residues Did Not Adsorb to DOPC. No changes in SHG signal with increasing aqueous peptoid concentrations were observed for the remaining four tripeptoids adsorbed to DOPC (chemical structures and calculated log $D_{7.4}$ values shown in Figure S9). These peptoids were differentiated from 4, 5, and 6 because they included either only one N1npm residue or two N-phenylmethyl glycine (Npm) aromatic residues. We measured similar molar extinction coefficients for peptoid 4 comprising

two N1npm residues and a peptoid with only a single N1npm residue (Figure S1). We suggest that the low SHG signal is not due to a lack of resonance enhancement from adsorbed peptoids, but instead to minimal adsorption. Without a second aromatic residue in the peptoid, the hydrophobicity was significantly lower (calculated log $D_{7.4}$ values ranged from -1.33 to -3.95, Figure S9); we speculate that lower hydrophobicity accounts for the binding behavior of peptoids shown in Figure S9 compared to 4, 5, and 6.

Adsorption of 3 to Charged Lipids in HEPES versus PBS Buffers Followed Different Trends. To better understand why adsorption of 1 and 3 to charged lipids did not follow the same trends, we monitored adsorption of 3 to DOPC, DOTAP (+), and DOPG (-) in an alternate buffer. Phosphate buffer has been shown to form "amorphous mesh multilayers" on anionic SLBs, 61 which may result in charge shielding or more complex electrostatic interactions. To eliminate the effects of phosphate buffer, we repeated binding experiments in 50 mM HEPES buffer at pH 7.4 and reported fit coefficients for 3 adsorbed to DOPC, DOTAP (+), and DOPG (-) in Figure 6. Previous studies suggest that HEPES

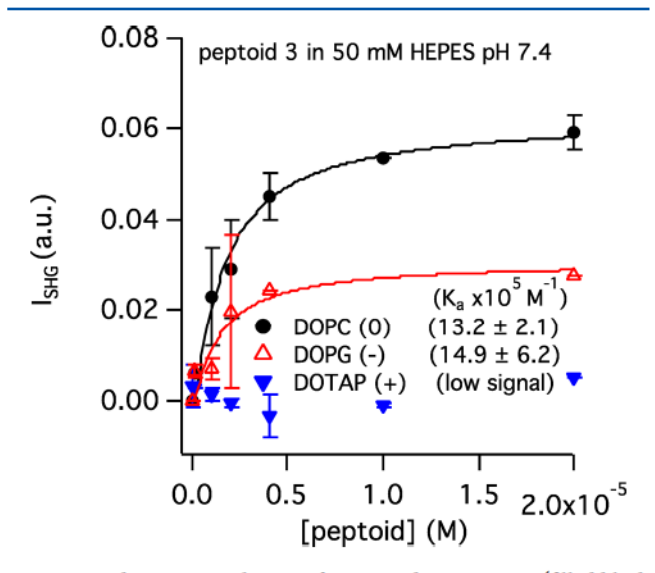


Figure 6. Adsorption isotherms of tripeptoid 3 to DOPC (filled black circles), DOPG (–) (empty red triangles), and DOTAP (+) (filled blue triangles). Equilibrium binding constants (K_a) are shown in parentheses. Experiments were conducted in 50 mM HEPES at pH 7.4 (ionic strength was maintained at 0.215 M with NaCl).

buffer has a lower capacity to screen the charge of lipid head groups compared to sodium ions. In HEPES buffer, tripeptoid 3, which has a net cationic charge, exhibited stronger adsorption to DOPG (–) compared to DOTAP (+) (Figure 6), which follows the same trends as those observed for 1. As PBS buffer more closely mimics the salt conditions

within the human body compared to HEPES buffer, we suggest that interactions between charged peptoids and plasma membranes of cells with high content of charged lipids (such as brain tissue) may not follow trends predicted by electrostatics interactions.

Water-Soluble Peptoids Did Not Adsorb to Saturated Lipids. Peptoids 1 and 3 exhibited the highest surface coverages of all peptoids studied when adsorbed to DOPC but did not adsorb to DMPC (Figure S10). To the best of our knowledge, no other studies have reported adsorption of peptoid-bond-containing structures to gel-phase lipids. We suggest that no binding was previously observed and, therefore, not reported. These results were not surprising as peptoids with bulky aromatic side chains may intercalate more easily into the larger voids between disordered acyl chains in unsaturated DOPC compared to smaller gaps between wellordered, more tightly packed acyl chain hydrocarbons of saturated DMPC and DPPC.

CONCLUSIONS

In this study, we addressed the following question: How does adsorption to lipid membranes depend on peptoid sequence length and charge? We also quantified how changes in membrane composition, such as addition of charged lipids and cholesterol into fluid-phase lipid bilayers, impact peptoid-lipid interactions. We discovered five peptoid structures (1, 3, 4, 5, 6) that adsorbed to fluid-phase, zwitterionic lipid bilayers following the Langmuir model. None of the peptoids studied here adsorbed to gel-phase lipids. Peptoids 1, 3, 4, 5, and 6 exhibited higher K_a when adsorbed to DOPC w/CHO compared to DOPC only. The overall highest K_a value was attributed to interactions between the longest structure (1) adsorbed to DOPG (-) in PBS buffer pH 7.4. Studies of sequences with 15 (1), 6 (2), and 3 (3) total substituents revealed the importance of sequence length on peptoid-lipid interactions. Differences in reversibility of adsorption of 1 and 3 to DOPC were attributed to differences in sequence length, which impacted three-dimensional structure and hydrophobicity: 1 had a helical, self-associating structure while 3 was smaller, less hydrophobic, and had a higher charge density. Even though intermediate length 2 was more hydrophobic than 3 and exhibited high molar absorptivity, it did not adsorb to fluid-phase lipids bilayers, and we speculated that its regular three-dimensional structure contributed to this behavior. 41 Our studies suggest that there may be more than one mechanism governing peptoid-lipid interactions; these mechanisms are likely length- and hydrophobicity-dependent.

Tripeptoids are generally more water-soluble than longer peptoids and therefore highly relevant to potential applications of peptoids (ranging from biosensors to pharmaceutics), which involve aqueous environments. Ka values determined from adsorption to DOPC and DOPC w/CHO correlated strongly with tripeptoid hydrophobicities, as described by $\log D_{7.4}$ values, following the order 5 > 3 > 4 > 6. The net charges of tripeptoids were varied from most to least cationic in the order 3 = 4 > 5 > 6, and trends in I_{SHG}^{max} follow cationic charge. Electrostatic effects on adsorption to zwitterionic DOPC and DOPC w/CHO were probed, resulting in tripeptoids with the highest net cationic charge and hydrophobicities exhibiting the strongest binding interactions. We discovered that HEPES buffer pH 7.4 exhibited different trends in adsorption of tripeptoids to charged lipids. Cationic 3 exhibited stronger adsorption to DOPG (-) compared to DOPC(0) or DOTAP

(+) in HEPES buffer pH 7.4, likely due to interfering interactions between phosphate ions from PBS buffer and the anionic head groups on DOPG (-).

From this study, we learned a guiding principle for rational drug design: Small organic molecules with hydrophobic substituents and overall cationic charge will likely adsorb to and accumulate in zwitterionic, fluid-phase phospholipids. The insights gained here will inform predictions of mammalian plasma membrane accumulation of potential peptoid-based therapeutics. These principles may also be important when considering the potential physiological consequences of dissolution from peptoid-based coatings used in biosensor applications. With these molecular-level, quantitative descriptions in hand, we are now better prepared for the advent of peptoid-based medical technologies.

ASSOCIATED CONTENT

Supporting Information

The Supporting Information is available free of charge on the ACS Publications website at DOI: 10.1021/acs.jpcb.9b04641.

Peptoid characterization by high-resolution mass spectrometry and HPLC, derivation of simplified Langmuir model, UV-vis spectra of tripeptoids, chemical structures of the lipid components used in this study, polarization-dependent SHG experimental details and results, studies of peptoid desorption, fluorescence microscopy characterization of SLBs in the presence and absence of peptoids, chemical structures and $\log D_{7.4}$ values for tripeptoids which did not adsorb to DOPC, and complementary adsorption isotherm data (PDF)

AUTHOR INFORMATION

Corresponding Author

*E-mail: gstokes@scu.edu.

Author Contributions

^TM.R.L. and J.L.R. contributed equally. The manuscript was written through contributions of all authors. All authors have given approval to the final version of the manuscript.

Notes

The authors declare no competing financial interest.

ACKNOWLEDGMENTS

G.Y.S. gratefully acknowledges a Clare Boothe Luce professorship and a Cottrell Scholar Award from the Research Corporation for Scientific Advancement. A.A.F. acknowledges funding from the National Science Foundation CHE-1566604. J.L.R. was supported by a DeNardo Science Scholar Award. V.P.D. and K.M.D. were supported by Summer Research Awards from Dr. Richard Bastiani. G.Y.S. and A.A.F. acknowledge funds from a STEM Convergence grant provided by the Provost's Office at SCU. We thank other members of the Stokes lab, particularly Gigi Gadbois, for help with lipid and buffer preparation, occasional data collection, and conducting desorption and bare silica studies. We also thank Dr. Paul Abbyad, Bella Lynch, and Dan Horvath for help with fluorescence microscopy experiments and analysis.

REFERENCES

(1) Lundbæk, J. A.; Koeppe, R. E.; Andersen, O. S. Amphiphile regulation of ion channel function by changes in the bilayer spring constant. Proc. Natl. Acad. Sci. U. S. A. 2010, 107, 15427-15430.

- (2) Schreier, S.; Malheiros, S. V. P.; de Paula, E. Surface active drugs: self-association and interaction with membranes and surfactants. Physicochemical and biological aspects. *Biochim. Biophys. Acta, Biomembr.* 2000, 1508, 210–234.
- (3) Nunes, C.; Brezesinski, G.; Lima, J. L. F. C.; Reis, S.; Lucio, M. Effects of non-steroidal anti-inflammatory drugs on the structure of lipid bilayers: therapeutical aspects. *Soft Matter* 2011, 7, 3002–3010.
- (4) Coimbra, J. T. S.; Fernandes, P. A.; Ramos, M. J. Revisiting partition in hydrated bilayer systems. *J. Chem. Theory Comput.* 2017, 13, 2290–2299.
- (5) Kluever, N.; Vogs, C.; Altenburger, R.; Escher, B. I.; Scholz, S. Development of a general baseline toxicity QSAR model for the fish embryo acute toxicity test. *Chemosphere* 2016, 164, 164–173.
- (6) Paloncýová, M.; Berka, K.; Otyepka, M. Molecular insight into affinities of drugs and their metabolites to lipid bilayers. *J. Phys. Chem.* B 2013, 117, 2403–2410.
- (7) Rowe, E. S.; Zhang, F.; Leung, T. W.; Parr, J. S.; Guy, P. T. Thermodynamics of membrane partitioning for a series of n-alcohols determined by titration calorimetry: Role of hydrophobic effects. *Biochemistry* 1998, 37, 2430–2440.
- (8) Endo, S.; Escher, B. I.; Goss, K.-U. Capacities of membrane lipids to accumulate neutral organic chemicals. *Environ. Sci. Technol.* 2011, 45, 5912–5921.
- (9) Goss, K.-U.; Schwarzenbach, R. P. Linear free energy relationships used to evaluate equilibrium partitioning of organic compounds. *Environ. Sci. Technol.* 2001, 35, 1–9.
- (10) Zuckermann, R. N. Peptoid origins. Biopolymers 2011, 96, 545-555.
- (11) Zuckermann, R. N.; Kodadek, T. Peptoids as potential therapeutics. Curr. Opin. Mol. Ther. 2009, 11, 299-307.
- (12) Knight, A. S.; Zhou, E. Y.; Francis, M. B.; Zuckermann, R. N. Sequence programmable peptoid polymers for diverse materials applications. *Adv. Mater.* 2015, 27, 5665–5691.
- (13) Lau, K. H. A. Peptoids for biomaterials science. Biomater. Sci. 2014, 2, 627-633.
- (14) Kapoor, R.; Eimerman, P. R.; Hardy, J. W.; Cirillo, J. D.; Contag, C. H.; Barron, A. E. Efficacy of antimicrobial peptoids against Mycobacterium tuberculosis. *Antimicrob. Agents Chemother.* 2011, 55, 3058–3062.
- (15) Kapoor, R.; Wadman, M. W.; Dohm, M. T.; Czyzewski, A. M.; Spormann, A. M.; Barron, A. E. Antimicrobial peptoids are effective against Pseudomonas aeruginosa biofilms. *Antimicrob. Agents Chemother.* 2011, 55, 3054–3057.
- (16) Statz, A. R.; Meagher, R. J.; Barron, A. E.; Messersmith, P. B. New Peptidomimetic Polymers for Antifouling Surfaces. *J. Am. Chem. Soc.* 2005, 127, 7972–7973.
- (17) Chongsiriwatana, N. P.; Patch, J. A.; Czyzewski, A. M.; Dohm, M. T.; Ivankin, A.; Gidalevitz, D.; Zuckermann, R. N.; Barron, A. E. Peptoids that mimic the structure, function, and mechanism of helical antimicrobial peptides. *Proc. Natl. Acad. Sci. U. S. A.* 2008, 105, 2794—2799.
- (18) Chongsiriwatana, N. P.; Barron, A. E. Comparing bacterial membrane interactions of antimicrobial peptides and their mimics. *Methods Mol. Biol.* 2010, 618, 171–182.
- (19) Chongsiriwatana, N. P.; Wetzler, M.; Barron, A. E. Functional synergy between antimicrobial peptoids and peptides against Gramnegative bacteria. *Antimicrob. Agents Chemother.* 2011, 55, 5399–5402.
- (20) Statz, A. R.; Park, J. P.; Chongsiriwatana, N. P.; Barron, A. E.; Messersmith, P. B. Surface-immobilised antimicrobial peptoids. *Biofouling* 2008, 24, 439–448.
- (21) Turkett, J. A.; Bicker, K. L. Evaluating the effect of peptoid lipophilicity on antimicrobial potency, cytotoxicity, and combinatorial library design. ACS Comb. Sci. 2017, 19, 229–233.
- (22) Simon, R. J.; Kania, R. S.; Zuckermann, R. N.; Huebner, V. D.; Jewell, D. A.; Banville, S.; Ng, S.; Wang, L.; Rosenberg, S.; Marlowe, C. K. Peptoids: a modular approach to drug discovery. *Proc. Natl. Acad. Sci. U. S. A.* 1992, 89, 9367–9371.

- (23) Hebert, M. L.; Shah, D. S.; Blake, P.; Turner, J. P.; Servoss, S. L. Tunable peptoid microspheres: effects of side chain chemistry and sequence. *Org. Biomol. Chem.* 2013, 11, 4459–4464.
- (24) Trader, D. J.; Simanski, S.; Kodadek, T. Reversible and highly selective inhibitor of the proteasomal ubiquitin receptor Rpn13 is toxic to multiple myeloma cells. *J. Am. Chem. Soc.* 2015, 137, 6312–6319.
- (25) Lee, J.; Reddy, M. M.; Kodadek, T. Discovery of an orexin receptor positive potentiator. *Chem. Sci.* 2010, 1, 48-54.
- (26) Kölmel, K. D.; Fürniss, D.; Susanto, S.; Lauer, A.; Grabher, C.; Bräse, S.; Schepers, U. Cell penetrating peptoids (CPPos): Synthesis of a small combinatorial library by using IRORI MiniKans. *Pharmaceuticals* 2012, 5, 1265.
- (27) Dohm, M. T.; Kapoor, R.; Barron, A. E. Peptoids: bio-inspired polymers as potential pharmaceuticals. *Curr. Pharm. Des.* 2011, 17, 2732–2747.
- (28) Saini, A.; Verma, G. In *Nanostructures for Novel Therapy*; Ficai, D., Grumezescu, A. M., Eds.; Elsevier: 2017; pp 251-280.
- (29) Foged, C.; Franzyk, H.; Bahrami, S.; Frokjaer, S.; Jaroszewski, J. W.; Nielsen, H. M.; Olsen, C. A. Cellular uptake and membrane-destabilising properties of α -peptide/ β -peptoid chimeras: lessons for the design of new cell-penetrating peptides. *Biochim. Biophys. Acta, Biomembr.* 2008, 1778, 2487–2495.
- (30) Jing, X.; Kasimova, M. R.; Simonsen, A. H.; Jorgensen, L.; Malmsten, M.; Franzyk, H.; Foged, C.; Nielsen, H. M. Interaction of peptidomimetics with bilayer membranes: Biophysical characterization and cellular uptake. *Langmuir* 2012, 28, 5167–5175.
- (31) Najafi, H.; Servoss, S. L. Altering the edge chemistry of bicelles with peptoids. *Chem. Phys. Lipids* 2018, 217, 43–50.
- (32) Jing, X.; Yang, M.; Kasimova, M. R.; Malmsten, M.; Franzyk, H.; Jorgensen, L.; Foged, C.; Nielsen, H. M. Membrane adsorption and binding, cellular uptake and cytotoxicity of cell-penetrating peptidomimetics with α -peptide/ β -peptoid backbone: Effects of hydrogen bonding and α -chirality in the β -peptoid residues. *Biochim. Biophys. Acta, Biomembr.* 2012, 1818, 2660–2668.
- (33) Shen, Y. R. Optical Second Harmonic Generation at Interfaces. *Annu. Rev. Phys. Chem.* 1989, 40, 327–350.
- (34) Shen, Y. R. Surface contribution versus bulk contribution in surface nonlinear optical spectroscopy. *Appl. Phys. B: Lasers Opt.* 1999, 68, 295–300.
- (35) Guyot-Sionnest, P.; Shen, Y. R. Local and nonlocal surface nonlinearities for surface optical second-harmonic generation. *Phys. Rev. B: Condens. Matter Mater. Phys.* 1987, 35, 4420–4426.
- (36) Hedegaard, S. F.; Derbas, M. S.; Lind, T. K.; Kasimova, M. R.; Christensen, M. V.; Michaelsen, M. H.; Campbell, R. A.; Jorgensen, L.; Franzyk, H.; Cárdenas, M.; Nielsen, H. M. Fluorophore labeling of a cell-penetrating peptide significantly alters the mode and degree of biomembrane interaction. *Sci. Rep.* 2018, *8*, 6327.
- (37) Hughes, L. D.; Rawle, R. J.; Boxer, S. G. Choose your label wisely: Water-soluble fluorophores often interact with lipid bilayers. *PLoS One* 2014, 9, e87649.
- (38) Nguyen, T. T.; Sly, K. L.; Conboy, J. C. Comparison of the energetics of avidin, streptavidin, neutravidin, and anti-biotin antibody binding to biotinylated lipid bilayer examined by second-harmonic generation. *Anal. Chem.* 2012, 84, 201–208.
- (39) Stokes, G. Y.; Conboy, J. C. Measuring selective estrogen receptor modulator (SERM)—membrane interactions with second harmonic generation. J. Am. Chem. Soc. 2014, 136, 1409–1417.
- (40) Fearon, A. D.; Stokes, G. Y. Thermodynamics of indomethacin adsorption to phospholipid membranes. *J. Phys. Chem. B* 2017, 121, 10508–10518.
- (41) Fuller, A. A.; Yurash, B. A.; Schaumann, E. N.; Seidl, F. J. Self-association of water-soluble peptoids comprising (S)-N-1-(naphthylethyl)glycine residues. *Org. Lett.* 2013, *15*, 5118–5121.
- (42) Jimenez, C. J.; Tan, J.; Dowell, K. M.; Gadbois, G. E.; Read, C. A.; Burgess, N.; Cervantes, J. E.; Chan, S.; Jandaur, A.; Karanik, T.; et al. Peptoids advance multidisciplinary research and undergraduate education in parallel: Sequence effects on conformation and lipid interactions. *Biopolymers* 2019, 110, e23256.

- (43) Kalb, E.; Frey, S.; Tamm, L. K. Formation of supported planar bilayers by fusion of vesicles to supported phospholipid monolayers. *Biochim. Biophys. Acta, Biomembr.* 1992, 1103, 307–316.
- (44) Calkins, A. L.; Yin, J.; Rangel, J. L.; Landry, M. R.; Fuller, A. A.; Stokes, G. Y. A thermodynamic description of the adsorption of simple water-soluble peptoids to silica. *Langmuir* 2016, 32, 11690–11697.
- (45) Corn, R. M.; Higgins, D. A. Optical second harmonic generation as a probe of surface chemistry. *Chem. Rev.* 1994, 94, 107–125.
- (46) Langmuir, I. The adsoprtion of gases on plane surfaces of glass, mica and platinum. J. Am. Chem. Soc. 1918, 40, 1361–1403.
- (47) Nguyen, T. T.; Conboy, J. C. High-throughput screening of drug—lipid membrane interactions via counter-propagating second harmonic generation imaging. *Anal. Chem.* 2011, 83, 5979—5988.
- (48) Fuller, A. A.; Tenorio, K.; Huber, J.; Hough, S.; Dowell, K. M. A peptoid supramolecular host for benzo[a]pyrene in water. Supramol. Chem. 2018, 30, 336–344.
- (49) Campen, R. K.; Zheng, D.-s.; Wang, H.-f.; Borguet, E. Second harmonic generation as a probe of multisite adsorption at solid—liquid interfaces of aqueous colloid suspensions. *J. Phys. Chem. C* 2007, 111, 8805—8813.
- (50) Ishiguro, R.; Matsumoto, M.; Takahashi, S. Interaction of fusogenic synthetic peptide with phospholipid bilayers: Orientation of the peptide α -helix and binding isotherm. *Biochemistry* **1996**, 35, 4976–4983
- (51) Cseh, R.; Benz, R. The adsorption of phloretin to lipid monolayers and bilayers cannot be explained by Langmuir adsorption isotherms alone. *Biophys. J.* 1998, 74, 1399–1408.
- (52) Yan, E. C.; Eisenthal, K. B. Effect of cholesterol on molecular transport of organic cations across liposome bilayers probed by second harmonic generation. *Biophys. J.* 2000, 79, 898–903.
- (53) Hung, W.-C.; Lee, M.-T.; Chen, F.-Y.; Huang, H. W. The condensing effect of cholesterol in lipid bilayers. *Biophys. J.* 2007, 92, 3960–3967.
- (54) van Duyl, B. Y.; Meeldijk, H.; Verkleij, A. J.; Rijkers, D. T. S.; Chupin, V.; de Kruijff, B.; Killian, J. A. A Synergistic effect between cholesterol and tryptophan-flanked transmembrane helices modulates membrane curvature. *Biochemistry* 2005, 44, 4526–4532.
- (55) Holt, A.; de Almeida, R. F. M.; Nyholm, T. K. M.; Loura, L. M. S.; Daily, A. E.; Staffhorst, R. W. H. M.; Rijkers, D. T. S.; Koeppe, R. E.; Prieto, M.; Killian, J. A. Is there a preferential interaction between cholesterol and tryptophan residues in membrane proteins? *Biochemistry* 2008, 47, 2638–2649.
- (56) Orädd, G.; Schmidtchen, A.; Malmsten, M. Effects of peptide hydrophobicity on its incorporation in phospholipid membranes an NMR and ellipsometry study. *Biochim. Biophys. Acta, Biomembr.* 2011, 1808, 244–252.
- (57) Smith, K. A.; Gale, B. K.; Conboy, J. C. Micropatterned fluid lipid bilayer arrays created using a continuous flow microspotter. *Anal. Chem.* 2008, *80*, 7980–7987.
- (58) Lapinski, M. M.; Castro-Forero, A.; Greiner, A. J.; Ofoli, R. Y.; Blanchard, G. J. Comparison of liposomes formed by sonication and extrusion: Rotational and translational diffusion of an embedded chromophore. *Langmuir* 2007, 23, 11677–11683.
- (59) Richter, R. P.; Bérat, R.; Brisson, A. R. Formation of solid-supported lipid bilayers: An integrated view. *Langmuir* 2006, 22, 3497–3505.
- (60) ChemAxon. MarvinSketch, version 19.10; 2019. http://www.chemaxon.com.
- (61) Trewby, W.; Livesey, D.; Voïtchovsky, K. Buffering agents modify the hydration landscape at charged interfaces. *Soft Matter* 2016, 12, 2642–2651.